Real-Time Detection of Internal Short Circuits in Lithium-Ion Batteries using an Extend Kalman Filter: A Novel Approach Combining Electrical and Thermal Measurements

Yiqi Jia[1], Lorenzo Brancato[1], Marco Giglio[1], and Francesco Cadini[1,*]

[1] *Politecnico di Milano, Department of Mechanical Engineering, Via La Masa 1, 20156, Milan, Italy*
yiqi.jia@polimi.it
lorenzo.brancato@polimi.it
marco.giglio@polimi.it
**Corresponding author: francesco.cadini@polimi.it*

ABSTRACT

Concerns over fuel scarcity and environmental degradation largely drive the increasing popularity of electric vehicles (EVs). Lithium-ion batteries (LIBs), known for their high energy and power densities, are the favored power source for EVs. Over the past few decades, research has been concentrated on ensuring these batteries operate efficiently, safely, and reliably. A key issue impacting the safety of Li-ion batteries is thermal runaway (TR), which can lead to hazardous battery fires. Internal short circuits (ISCs) are often the primary cause of these TR incidents, making the early detection of spontaneous ISC formation a pivotal diagnostic task. This research introduces an innovative ISC detection technique for cylindrical Li-ion battery cells. This technique is based on the augmentation of the model state vector in an extended Kalman filter (EKF), combining both classical voltage measurements to surface temperature observations. This framework enables real-time estimation of the internal ISC state while maintaining computational efficiency. The proposed method is tested numerically considering a high-fidelity numerical plant cycled using charge-depleting tests that mimic a practical battery cell working cycle at various C rates and at different ambient temperatures to account for both load and environmental uncertainties. The results demonstrate the robustness and effectiveness of the method. In addition, the method has been proven to be computationally efficient, demonstrating the feasibility of its real-time implementation.

1. INTRODUCTION

Global warming and air pollution have spurred the recent growth of the EV market. Among various battery types, LIBs have gained widespread popularity as portable energy sources for EVs due to their notable advantages, including high energy density, high power density, and long lifetime (Goodenough & Kim, 2010). However, irreversible processes, such as the formation of a solid-electrolyte interphase (SEI) during LIBs charging and discharging cycles, can adversely affect battery health, leading to continuous capacity degradation and an increased risk of battery failures and severe safety issues, such as TR accidents (Amine, Kanno, & Tzeng, 2014). Given that ISC has been identified as the primary cause of TR fire accidents, preventing severe ISC is crucial for the Battery Management System (BMS) to ensure the safe and reliable operation of EVs (Grabow et al., 2023).

While the complete understanding of the spontaneous ISC formation mechanism in rechargeable batteries remains elusive, it has been observed that ISC progression typically involves three stages: the early stage, the middle stage, and the late stage (G. Zhang et al., 2021). During the early and middle stages, the voltage drop and temperature increase may be used as valuable indicators to detect ISC and prevent TR. However, the minimal signal changes in thermal and electrical indicators pose challenges in detecting faults based on raw measurements. In contrast, during the late stage, the rapid signal changes make it too late for alarms to counter the fast-changing signals.

Over the past few years, there has been a significant effort by many researchers to develop and integrate diagnostic algorithms to detect ISC and prevent TR. Several data-driven methods have been proposed, which are based on parameter inconsistency. These include methods based on voltage (Gao et al., 2021), temperature (Sun, Chou, Shieh, & Chu, 2021), State of Charge (SoC) (Lai et al., 2021), and remaining charging capacity (RCC) (Kong et al., 2018). As previously discussed, the inherent alterations in electro-thermal signals caused by spontaneous ISC formation may not be immedi-

https://doi.org/10.36001/IJPHM.2024.v15i3.3848

ately distinguishable in the dynamic responses of the battery, particularly during the incipient stages of ISC. Furthermore, signal fluctuations attributable to external factors could potentially trigger unwarranted alarms. Consequently, the precise determination of an appropriate threshold value poses a significant challenge, given that this value profoundly influences the promptness and accuracy of detection.

Other data-driven approaches that leverage the power of machine learning techniques have also been developed recently. These approaches employ models such as deep neural networks (Naha et al., 2020) or random forest (Xiao & Xiao, 2021). However, being only based on data, the performance of these approaches is strongly limited by the scarcity of available data and the challenges in generating new ones.

Lastly, the detection of ISC can also be achieved by utilizing battery cell models. These include Equivalent Circuit Models (ECM) (M. X. Zhang et al., 2018; Seo, Park, Song, & Kim, 2020; Asakura, Nakashima, Nakatsuji, & Fujikawa, 2010, 2012; Feng, He, Lu, & Ouyang, 2018), or more advanced electro-chemical models (Ma, Deng, & Wang, 2023). However, most of these works only rely on the electrical modeling of the battery cell or consider electrical and thermal dynamics separately. As mentioned before, temperature plays a crucial role in spontaneous ISC formation, hence using a coupled electro-thermal model of the battery cell is a potentially more effective approach. Nevertheless, research on model-based algorithms that combine both electrical and thermal measurements for ISC detection remains relatively limited in the literature. The latter measurements are typically available in commercial BMS, and in fact, some model-based algorithms considering an electro-thermal model of a battery cell for SoC estimation have recently been reported in the literature (Qin, Che, Li, Cai, & Jiang, 2022; X. Liu et al., 2024; Saqli, Bouchareb, M'sirdi, & Bentaie, 2023). This suggests that a model-based framework considering an electro-thermal model of a battery cell could also be used for ISC detection, and more importantly, given the non-negligible effect of ISC on battery temperature dynamics, combining both voltage and temperature measurements is promising for improving ISC detection performance.

Based on a previous work by the same authors (Jia, Brancato, Giglio, & Cadini, 2024), this study introduces a novel model-based ISC detection approach that employs the EKF algorithm to track the ISC state evolution in real-time. The algorithm utilizes the input load current and the voltage and surface temperature measurements to dynamically update the state of its model, which is augmented with a variable directly related to ISC. In comparison with other ISC detection approaches, this approach has the following advantages:

- it relies on both voltage and temperature observations to more accurately update the dynamic state evolution of the cell;
- it considers a quantity strongly related to ISC in the model state, allowing detection and quantification of ISC.

Moreover, as demonstrated in this work, the algorithm has been designed to meet the computational and accuracy requirements necessary for its implementation in a BMS. It is based on a simple electro-thermal battery cell model, which only marginally increases the computational complexity, and on an efficient and lean filtering algorithm.

In our previous work (Jia et al., 2024), we had already demonstrated the method's advantages in quicker and more accurate detection compared to classical model-based approaches only relying on electrical measurements. This is further demonstrated in this study when considering a more realistic plant by implementing a coupled electro-thermal model of a cylindrical battery cell. This model has been validated experimentally in a previous work by Lin et al. (Lin et al., 2014), and is employed to accurately simulate the electrical and thermal responses of the cell under varying ISC conditions. The simulated signals are then fed to the EKF-based algorithm, which performs the online ISC state estimation. In addition, this study tests the robustness and reliability of this approach numerically. The effectiveness of the algorithm is demonstrated by considering different load and environmental conditions. The latter affects the heat generation and consequently, the dynamics coupling of the cell, which depends on its core temperature. This dynamic coupling is due to the fact that the electrical parameters, which exhibit temperature-dependent variation in the plant, remain largely unaffected when the cell temperature variations are small, while they undergo considerable alteration when the core cell temperature variations are significant.

The remainder of the paper is organized as follows: Section 2 presents a brief overview of the coupled electro-thermal model of a cylindrical battery cell, which was utilized to test the algorithm; Section 3 outlines the online ISC detection algorithm based on EKF; Section 4 illustrates the algorithm's detection performance; finally, Section 5 draws out the conclusions from this work and suggests potential future developments.

2. COUPLED ELECTRO-THERMAL BATTERY MODEL

This section briefly reviews the coupled electro-thermal model of a cylindrical LIB cell developed by Lin et al. (2014). In this model, the terminal voltage dynamic is captured using an ECM, while the core and surface temperatures of the cell are estimated with a two-state thermal model. The ECM submodel is modified adding a resistance in parallel to the output terminals of the circuit to model the ISC occurrence. The electrical parameters depend on the core temperature, SoC, and current flow direction; the thermal parameters are assumed constant instead.

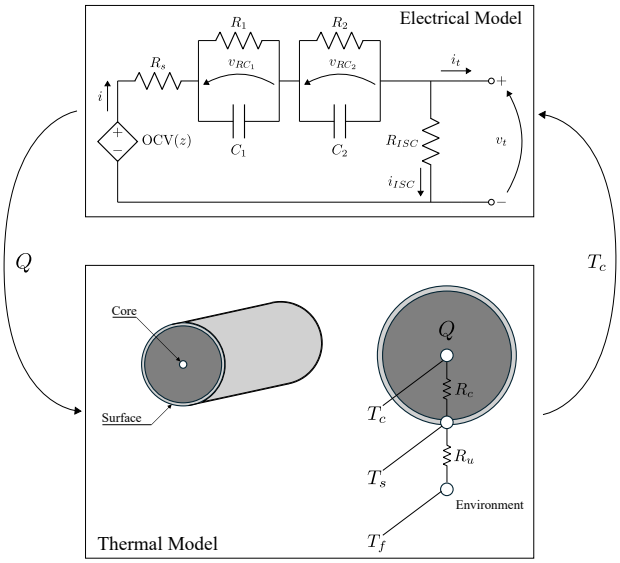

Figure 1. Coupled electro-thermal model of a cylindrical battery cell.

2.1. Electrical modelling

At the top of Figure 1, which depicts the schematic of the coupled electro-thermal model, the electrical submodel is illustrated as a second-order ECM. Under a current i (positive when discharging), the terminal voltage, denoted with v_t is obtained according to the Kirchhoff laws:

$$v_t = \mathrm{OCV}(z) - R_s i - v_{RC_1} - v_{RC_2} \tag{1}$$

The first term, $\mathrm{OCV(z)}$, is the so-called open circuit voltage, which is a non-linear function of the SoC, according to the empirical relationship taken from Lai et al. (2021) and shown in Figure 2. The SoC is denoted with z in the model, and it is calculated via the Coulomb counting equation (Chang, 2013):

$$\frac{dz}{dt} = -\frac{1}{C_{bat}} i \tag{2}$$

where C_{bat} is the battery nominal capacity, expressed in As. The second term in Eq. (1) is the voltage drop across the internal series resistance R_s. The last two terms, v_{RC_1} and v_{RC_2}, are the voltage drops across the two series of parallel RC circuits, which are used to model the transients voltage dynamics (G. Liu et al., 2014). Their evolution is described as

$$\frac{dv_{RC_1}}{dt} = -\frac{1}{R_1 C_1} v_{RC_1} + \frac{1}{C_1} i \tag{3}$$

$$\frac{dv_{RC_2}}{dt} = -\frac{1}{R_2 C_2} v_{RC_2} + \frac{1}{C_2} i \tag{4}$$

where R_1 and R_2 are the equivalent polarization resistances, and C_1 and C_2 are the equivalent polarization capacitances. The current i flowing within the circuit elements, according to the Kirchhoff laws, is the sum of two contributions:

$$i = i_t + i_{ISC} \tag{5}$$

being i_t the load current, and $i_{ISC} = v_t / R_{ISC}$ the parasitic current due to ISC.

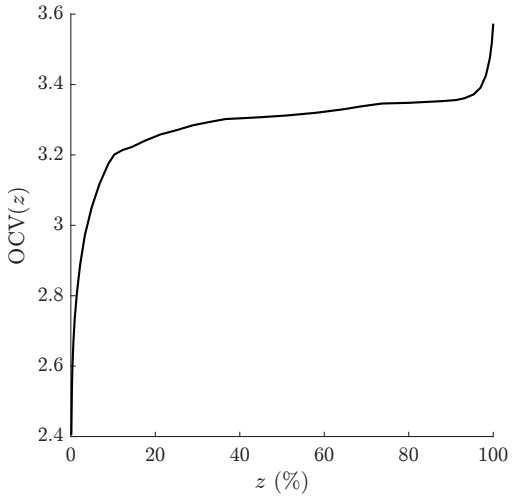

Figure 2. Average voltage-SoC curve under C/20 discharging tests. Adapted from Lai et al. (2021).

2.2. Thermal modelling

Assuming longitudinal homogeneity, the lumped thermal dynamics of a cylindrical battery cell can be represented by a two-state thermal model, which is illustrated at the bottom of Figure 1.The governing equations of the core temperature, T_c, and the surface temperature, T_s are (Lin et al., 2012; Park & Jaura, 2003):

$$C_c \frac{dT_c}{dt} = Q + \frac{T_s - T_c}{R_c} \tag{6}$$

$$C_s \frac{dT_s}{dt} = \frac{T_f - T_s}{R_u} - \frac{T_s - T_c}{R_c} \tag{7}$$

The heat generated, denoted in Eq. (6) with Q, is due to the chemical reactions taking place in the electrode assembly during the battery operation. This quantity can be estimated based on the electrical model (Lin et al., 2014), as

$$Q = i\left(\mathrm{OCV}(z) - v_t\right) \tag{8}$$

which accounts for the joule heating and the energy that is dissipated in the electrode overpotentials (Bernardi, Pawlikowski,

& Newman, 1985). To model heat generation more accurately, reversible heat, i.e., entropic heat, could be also incorporated in the model (Gu & Wang, 2000). A heat conduction resistance, R_c, is employed to mimic the heat exchange occurring between the core and the surface; convective cooling through the battery surface is instead modeled with a convective resistance, R_u, between the battery surface and the environment (whose temperature is denoted with T_f). Finally, the core heat capacity, C_c, and the surface heat capacity, C_s, determine the rate-of-change of T_c and T_s, respectively.

2.3. Electro-thermal coupling

The value of R_s is strongly dependent on temperature and current flow direction and only slightly dependent on SoC, hence it can be modeled with an Arrhenius-like function (Lin et al., 2014):

$$R_s^j = R_{s,0}^j \exp\left(\frac{T_{\text{ref},R_s}^j}{T - T_{\text{shift},R_s}^j}\right) \tag{9}$$

with $j = d, c$ when discharging or charging, respectively.

Instead, the values of R_i and C_i vary with SoC, current flow direction, and temperature. For the polarization resistances a second-order polynomial function and an Arrhenius-like function are employed to respectively approximate SoC and temperature dependency (Lin et al., 2014):

$$R_i^j = \left(R_{i,0}^j + a_{i,1}^j z + a_{i,2}^j z^2\right) \exp\left(\frac{T_{\text{ref},R_i}^j}{T - T_{\text{shift},R_i}^j}\right) \tag{10}$$

with $i = 1, 2$ and $j = d, c$ when discharging or charging, respectively.

The polarization capacitances, instead, are fitted by a quadratic function of SOC affine with temperature (Lin et al., 2014):

$$\begin{aligned} C_i^j =& C_{i,0}^j + c_{i,1}^j z + + c_{i,2}^j z^2 + \\ & \left(c_{i,3}^j + c_{i,4}^j z + c_{i,t}^j z^2\right) T \end{aligned} \tag{11}$$

with $i = 1, 2$ and $j = d, c$ when discharging or charging, respectively.

The value of the coefficients in Eq. (9)-(11) are determined fitting the experimental data given in Lin et al. (2014). The value of all the other model parameters, which are assumed to be constant, are indicated in Table 1.

As detailed in Figure 1, the two sub-models interact through a two-way coupling. First, the electrical submodel computes the SoC and the voltage of the battery, based on the load current i_t and the electrical parameters. The difference between v_t and $\text{OCV}(z)$, along with i, is used to compute the electrical heat Q. Then, the thermal model calculates T_c and T_s based on Q and the environment temperature T_f. The core temperature, T_c, which represents the temperature of the lumped electrode assembly, is used to determine the value of the temperature-dependent parameters of the electrical model.

Parameter name	Symbol	Value	Unit
Nominal battery capacity	C_{bat}	2.1	Ah
Environment temperature	T_f	25	°C
Surface heat capacity	C_s	4.5	JK^{-1}
Core heat capacity	C_c	62.7	JK^{-1}
Heat conduction resistance	R_c	1.94	KW^{-1}
Heat convection resistance	R_u	3.19	KW^{-1}

Table 1. Constant model parameters.

The coupled electro-thermal model of a cylindrical LIB cell, which incorporates a representation of the ISC phenomenon, will henceforth be referred to as the cET-ISC model.

3. ONLINE ISC ESTIMATION ALGORITHM

The state of a dynamical system is a set of variables that fully describe the actual condition and behaviour of the system. Non-linear dynamical systems are systems whose dynamics depend on the state in a non-linear way, meaning that they cannot be expressed as a linear combination of the state variables (Walcott & Zak, 1987). A state-space model is a way of representing the dynamics and the observations of a system using a hidden state vector, which collects all the state variables (Nise, 2020). The state equation, denoted with f, and the observation equation, denoted with h, are two functions that define a state-space model. The state equation f describes how the state vector evolves as a function of the previous state and some noise. The observation equation h, instead, describes how the observed data is related to the state vector and some noise.

The EKF is a type of online state estimator. It is an iterative method that can estimate the state of non-linear dynamical systems (Simon, 2006). It deals with non-linearity by approximating the non-linear dynamic equations with linear ones using Taylor expansion. The algorithm has two main steps:

- the prediction step, where the next state estimate, denoted with $\hat{\mathbf{x}}$, and the predicted observations, denoted with $\hat{\mathbf{y}}$, are computed by using the previous state estimate in the non-linear dynamic equation and in the non-linear observation equation, respectively; also, in this step, the error covariance matrix, denoted with $\Sigma_{\hat{\mathbf{x}}}$, which represents the prediction uncertainty, is calculated;
- the correction step, where the state estimate and the error covariance matrix are updated with appropriately weighted

innovation terms that depend on the actual observations of the system.

The whole algorithm is shown in Table 2. Note that the algorithm must be properly initialized, assigning a value to the state vector estimate and the error covariance matrix, respectively.

The EKF algorithm is employed to perform parameter identification when the system parameters are unknown or uncertain and need to be estimated along with the state variables. Parameter identification is the process of finding the values of the parameters that best fit the observed data and the system model. The EKF can perform parameter identification by using one of the following methods (J. Zhang, Zhou, & Huang, 2018):

- Joint estimation: this method combines the state and parameter vectors into an augmented state vector, and the EKF estimates both the state and the parameters simultaneously. This method is simple and effective, but it may suffer from observability issues and high computational costs, especially when the augmented state dimension is big.
- Dual estimation: this method uses two separate EKFs, one for state estimation and one for parameter estimation. The state EKF uses the parameter estimates from the parameter EKF as inputs, and the parameter EKF uses the state estimates from the state EKF as outputs. This method is more efficient, but less accurate as it neglects possible cross-correlation effects between the state variables.

In this work, a simplified version of cET-ISC model described in Section 2, which neglects the electro-thermal coupling, is discretized in time using the forward Euler integration method, allowing its implementation in the filter. Following the approach employed by the same authors in a previous work (Jia et al., 2024), the state vector of the simplified model is augmented including the equivalent ISC conductance $G_{ISC} = 1/R_{ISC}$, yielding:

$$\mathbf{x} = [z,\ v_{RC_1},\ v_{RC_2},\ G_{ISC},\ T_c,\ T_s]^T \tag{12}$$

to allow the joint estimation of a parameter directly related to the ISC status. The choice of using G_{ISC} in place of R_{ISC} is motivated by the simpler computation of the Jacobian matrices, which is required by the EKF algorithm. However, R_{ISC} can be easily calculated from G_{ISC}. The input vector and the output vector are

$$\mathbf{u} = [i_t,\ v_t]^T \tag{13}$$

$$\mathbf{y} = [v_t,\ T_s]^T \tag{14}$$

Extended Kalman Filter Algorithm
Initialization:
Initialize state estimate $\hat{\mathbf{x}}_0^-$ and error matrix covariance $\Sigma_{\hat{\mathbf{x}}_0^-}$
Prediction Step:
Predict the state estimate:
$\hat{\mathbf{x}}_k^- = f(\hat{\mathbf{x}}_{k-1}^+, \mathbf{u}_{k-1}, \bar{\mathbf{w}}_{k-1})$
Predict the observations:
$\hat{\mathbf{y}}_k = h(\hat{\mathbf{x}}_{k-1}^+, \hat{\mathbf{y}}_{k-1}, \mathbf{u}_{k-1}, \bar{\mathbf{n}}_{k-1})$
Predict the error covariance matrix:
$\Sigma_{\hat{\mathbf{x}}_k^-} = A_k \Sigma_{\hat{\mathbf{x}}_{k-1}^-} A_k^T + B_k \Sigma_{\mathbf{w}} B_k^T$
Correction Step:
Compute the Kalman gain matrix:
$K_k = \Sigma_{\hat{\mathbf{x}}_k^-} C_k^T (C_k \Sigma_{\hat{\mathbf{x}}_k^-} C_k^T + D_k \Sigma_{\mathbf{n}} D_k^T)^{-1}$
Update the state estimate:
$\hat{\mathbf{x}}_k^+ = \hat{\mathbf{x}}_k^- + K_k(\mathbf{y}_k - \hat{\mathbf{y}}_k)$
Update the error covariance matrix:
$\Sigma_{\hat{\mathbf{x}}_k^+} = \Sigma_{\hat{\mathbf{x}}_k^-} - K_k(C_k \Sigma_{\hat{\mathbf{x}}_{k-1}^-} C_k^T + D_k \Sigma_{\mathbf{n}} D_k^T) K_k^T$
Where:
$A_k = \frac{\partial f}{\partial \mathbf{x}}\big\|_{\hat{\mathbf{x}}_{k-1}^+, \mathbf{u}_{k-1}, \bar{\mathbf{w}}_{k-1}}$ $B_k = \frac{\partial f}{\partial \mathbf{w}}\big\|_{\hat{\mathbf{x}}_{k-1}^+, \mathbf{u}_{k-1}, \bar{\mathbf{w}}_{k-1}}$
$C_k = \frac{\partial h}{\partial \mathbf{x}}\big\|_{\hat{\mathbf{x}}_{k-1}^+, \mathbf{u}_{k-1}, \bar{\mathbf{n}}_{k-1}}$ $D_k = \frac{\partial h}{\partial \mathbf{n}}\big\|_{\hat{\mathbf{x}}_{k-1}^+, \mathbf{u}_{k-1}, \bar{\mathbf{n}}_{k-1}}$
and $\Sigma_{\mathbf{w}}$, $\Sigma_{\mathbf{n}}$ are the covariance matrices of the two independent, zero-mean, Gaussian processes **w** and **n**.

Table 2. Description of the Extended Kalman Filter algorithm.

assuming that the load current i_t, the terminal voltage v_t, and the surface temperature T_s are all measurable quantities.

4. CASE STUDY

This section presents a numerical case study to demonstrate the effectiveness of the proposed algorithm in detecting and quantifying ISC insurgence for different operating conditions. These conditions encompass both low and high discharging and charging current profiles and different environmental temperatures. This allows for the assessment of the robustness of the online ISC estimation algorithm described in Section 3 against loads and environmental uncertainties. In addition, we have demonstrated the advantages of adding surface temperature measurements for enhanced ISC detection performance and the real-time feasibility of the approach.

In this section, the cET-ISC model previously described in Section 2 is employed to simulate the behaviour of an actual battery cell, generating voltage and surface temperature data. These data are then processed by the suggested EKF-based diagnostic tool to estimate the actual ISC state. For the remainder of this section, we refer to this model as the 'plant'.

4.1. ISC detection threshold

The selection of an appropriate ISC detection threshold, which is essential for the prompt triggering of an alarm and the ensuring of the safe operation of the battery, is largely contingent upon the specific type of battery and its intended application. Consequently, it is not feasible to determine such a

threshold in a non-case-specific manner. Nonetheless, in this work we proposed a systematic approach based on a preliminary analysis conducted in the plant, which could be replicated experimentally on a real battery cell to set an appropriate ISC detection threshold. This analysis involves the performance of a series of simple discharging and charging tests (at a current of 1C) with varying equivalent ISC resistances and at different ambient temperatures. From the observed voltage and temperature data, it is possible to compute some useful indicators, namely the discharge time t_{dis}, the charge time t_{ch}, and the maximum surface temperature $T_{s,\max}$, which are correlated with the presence of ISC, as previously demonstrated in Feng, Ouyang, et al. (2018). These quantities are highlighted in Figure 3. The analysis also involves an investigation into the extent to which the voltage and temperature measurements are affected. The results obtained are presented in Figure 4, where the indicators have been normalized with respect to the value obtained in nominal conditions, i.e., no ISC presence and ambient temperature of 25°C. For the considered ambient temperature range, the indicators derived from the electrical signals are minimally affected by the ambient temperature (the curves obtained at different temperatures overlap) but are strongly influenced by ISC severity. As expected, instead, the indicator derived from the temperature signal is mostly affected by the ambient temperature, especially when high values of the equivalent ISC resistance are considered, therefore we will use the charge and the discharge times as valuable indicators to set a proper ISC detection threshold.

The acceptable variance range of the nominal discharge and charge time of a LIB cell may vary depending on several factors such as the specific application, the health of the battery cells, the ambient temperature, and the load conditions. Here we conservatively set this range at ±5% of the nominal value. This is because, in the context of the anomaly under consideration, we favour the earliness of detection. However, a wider range could be employed to minimise the chances of triggering false alarms. The previous analysis therefore allows us to determine when the severity of the ISC in the plant becomes relevant by considering equivalent ISC values for which these quantities leave the acceptable variance range. Thus, as indicated by the dotted lines in Figure 4, if $R_{ISC} < 100\Omega$, the ISC can be neglected because its effect on the discharge and charge time is within the allowable variance range of these quantities. Therefore, we will set $R_{ISC} = 100\Omega$ as the detection threshold in our online ISC detection algorithm. Nonetheless, it is crucial to note that the proposed approach entails the continuous monitoring of the equivalent ISC resistance value, along with its temporal evolution. Consequently, if the value remains unchanging, the filter will converge on its true value. The ISC detection threshold proposed here is therefore only required to actually trigger an alarm, based on the aforementioned analysis. However, the user can observe that the equivalent ISC resistance value may have already decreased even before the alarm is triggered. This makes the overall approach less sensitive to the choice of the ISC detection threshold, as for a healthy cell, the estimated ISC resistance value is expected to oscillate around a very high value, which is the one at which the filter has been initialized, while for a faulty cell, a step decrease of the equivalent ISC resistance value is expected, as later shown in the results presented in Section 4.2.

As mentioned in the introduction, according to (G. Zhang et al., 2021) the ISC state can be classified based on how much it affects the electrical and thermal characteristics of the battery cell. Based on the previous analysis, the plant's electrical and thermal characteristics are slightly affected when $20\Omega \leq R_{ISC} < 100\Omega$ (variance 5-10%). This domain is therefore regarded as the soft ISC region. The plant's electrical and thermal characteristics are quite affected when instead $5\Omega < R_{ISC} \leq 20\Omega$ (variance 10-20%). This domain is therefore regarded as the moderate ISC region. Finally, the plant's electrical and thermal characteristics are severely affected when $R_{ISC} < 5\Omega$ (variance >20%). This domain is therefore regarded as the severe ISC region.

4.2. Detection results

The measurements processed by the suggested EKF-based diagnostic tool to estimate the actual ISC state, are generated by discharging and charging the plant, such that $0.1 \leq z \leq 0.9$, with a charge-depleting current profile followed by a constant charging current. Note that, to account for any dynamics that the plant does not capture (which include sensor noise, non-modeled electrochemical effects, e.g., hysteresis, as well as temperature gradient effects, since a two-state model is considered here, which can only capture the temperature difference between the cell core and surface), white noise is added to these measurements before being fed to the filter.

During the simulation, the plant is cycled with several working cycles, to allow the filter to converge to a steady-state value of the estimate. The working cycle shape considered is illustrated in Figure 5. The figure illustrates two profiles, with average discharging currents and constant charging currents of 1C and 4C. As a consequence of the overall lower current amplitude, the working cycle characterised by lower currents will generate, according to Eq (8), less electrical heat and hence will lead to a lower temperature variation in the battery cell core. Consequently, the dynamics coupling will be less pronounced in the former case, as the temperature-varying electrical parameters in the plant will be largely unaffected. This allows testing the robustness of the ISC detection algorithm presented in Section 3 against different load conditions.

A simplified electro-thermal model is employed within the filter for the sake of simplicity and computational efficiency.

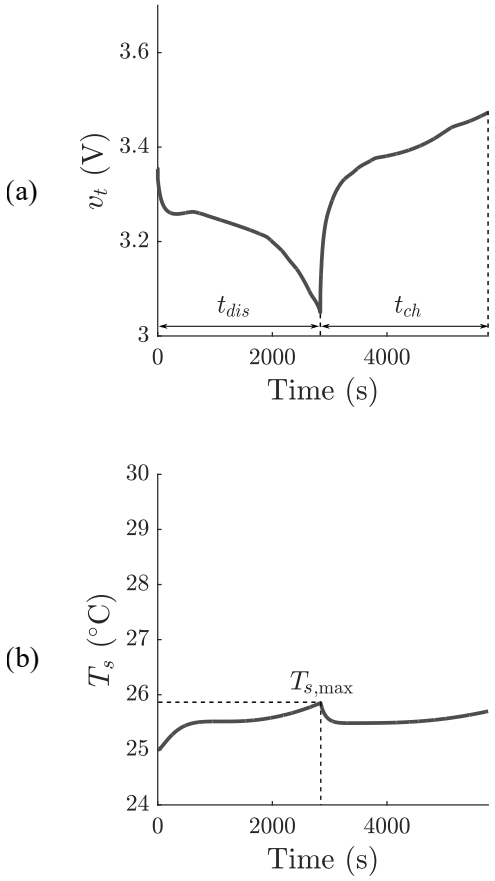

Figure 3. ISC severity indicators obtained from measurement signals. These outputs are obtained at the nominal plant condition, i.e., when no ISC is present and at the ambient temperature of 25°C, discharging/charging the plant with 1C current. (a) Terminal voltage. (b) Surface temperature.

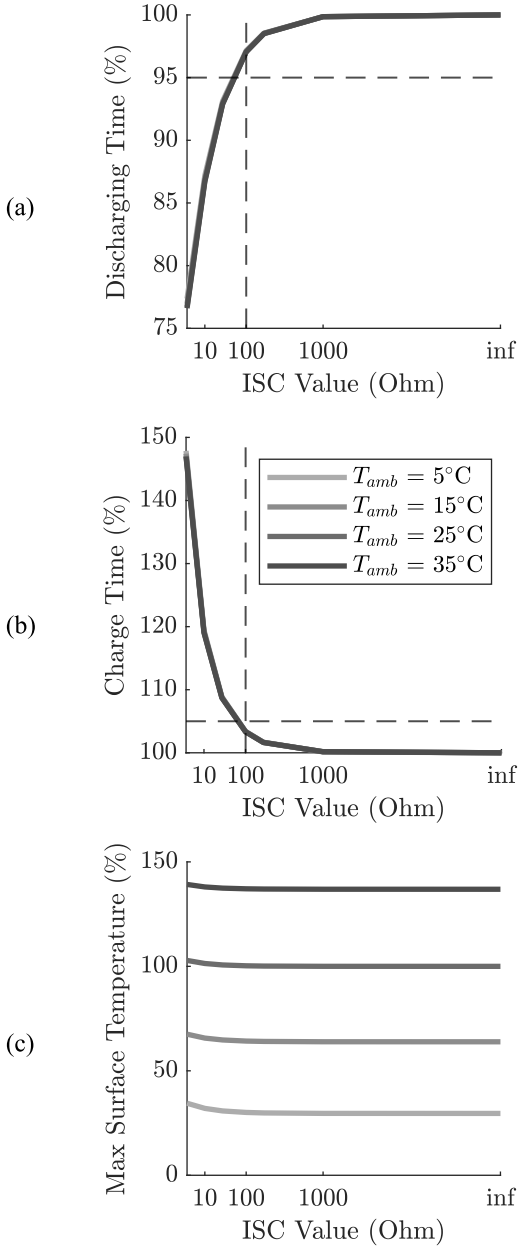

Figure 4. ISC indicators evolution with increasing ISC severity and variable ambient temperature. The dotted lines indicate the ISC value for which the allowed variance range ($\pm$ 5%) is overcome. These results have been obtained by discharging/charging the plant with 1C current. (a) Normalized discharge time. (b) Normalized charge time. (c) Normalized maximum surface temperature.

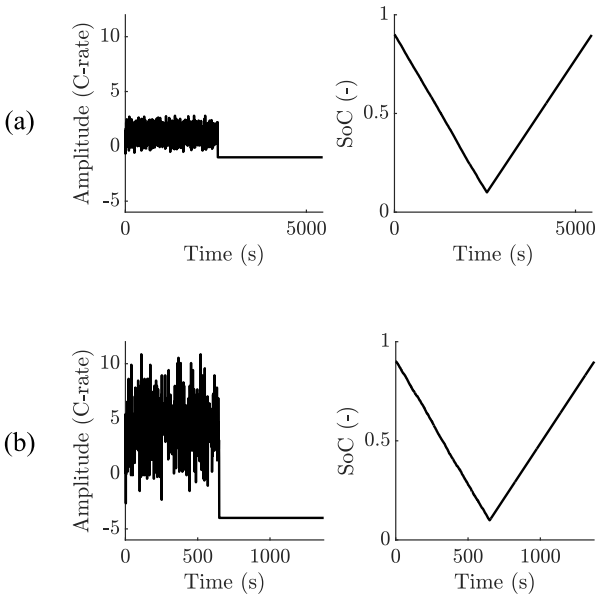

Figure 5. Single working cycle architecture (load current, on the left, and corresponding SoC evolution, on the right). The SoC outputs illustrated are obtained at the nominal plant condition, i.e., when no ISC is present and at the ambient temperature of 25°C. (a) Average 1C discharging/charging current. (b) Average 4C discharging/charging current.

This model does not consider the coupling between electrical and thermal dynamics, but includes constant electrical parameters estimated when the cell is at the nominal ambient temperature of 25°C. This simplification is adopted due to the practical constraints in real-world applications, where predicting the temperature range in which the battery cell will function is not always feasible. Moreover, conducting a comprehensive analysis of the cell dynamics evolution under varying environmental conditions can be a time-consuming and costly process.

The filter state estimate and error covariance matrix are initialized as follows:

$$\hat{\mathbf{x}}_0 = [0.90,\ 0\text{V},\ 0\text{V},\ 1/500\,\Omega^{-1},\ 298.15\text{K},\ 298.15\text{K}]^{\mathrm{T}}$$

$$\begin{aligned}\Sigma_{\hat{\mathbf{x}}_0} =&[10^{-6},\ 10^{-6}\text{V}^2,\ 10^{-6}\text{V}^2,\\ &10^{-8}\Omega^{-2},\ 10^{-6}\text{K}^2,\ 10^{-6}\text{K}^2]^{\mathrm{T}}\end{aligned}$$

where a negligible ISC condition is considered, i.e., $R_{ISC,0} > 100\Omega$. All the other filter parameters are indicated in Table 3. Note that the process noise covariance is non-zero only for the state variable we are interested in estimating, which is the equivalent ISC conductance. In other words, in the filter model, an additive process noise with standard deviation σ_G has been added only for the equivalent ISC conductance state, to allow the filter to dynamically update its value, and hence estimate its unknown evolution.

Parameter name	Symbol	Value	Unit
Sampling time	Δt	1	s
Voltage noise covariance	σ_V^2	5×10^{-5}	V^{-2}
Temperature noise covariance	σ_T^2	5×10^{-3}	K^{-2}
Process noise covariance	σ_G^2	5×10^{-11}	Ω^{-1}

Table 3. Filter parameters.

Before evaluating the algorithm's robustness against load conditions and environmental uncertainties, we compare the online ISC estimation algorithm performance in terms of timeliness of the detection when the latter is fed with solely voltage measurements and a combination of voltage and surface temperature measurements. The detection results obtained while cycling the plant with the working cycles with 1C current at different ISC conditions are illustrated in Figure 6. It should be noted that ISC detection can be initiated by setting a suitable threshold on the estimated ISC resistance value. In this work, this value is established at 100 Ω based on the analysis conducted in Section 4.1. An alarm is triggered at any time that the equivalent ISC estimate crosses downward the detection threshold, indicating the presence of an ISC. Therefore, the timeliness of the detection can be quantified as the time when this threshold is crossed, and the alarm is triggered. The results demonstrate how consistently, for different ISC severity, the timeliness increases when combined measurements are considered.

In the following, a comparison of the detection results, when working cycles with low and high current loads are considered, is carried out to understand the extent to which the load uncertainties affect the dynamics coupling in the plant and subsequently the detection performance for different ISC conditions. The detection results obtained while cycling the plant with the working cycles with low and high current at different ISC conditions are illustrated in Figure 7. Regardless of the strength of the dynamic coupling in the plant, the results show that the filter is capable of converging to a steady-state value of the equivalent ISC resistance. However, as expected, the coupling has a significant impact on the detection performance, especially when the ISC is soft. In this case, indeed, the large fluctuations in the response may led to false alarms. These fluctuations are due to the fact that the residuals between the predicted filter outputs and the measured outputs are significantly affected by the prediction errors. The latter are the result of the strong dynamics coupling in the plant, which affects the electrical parameters. As the ISC becomes more severe, its impact on the residuals increases and becomes comparable in amplitude to one of the mismodelling effects, or even greater, allowing the filter to better estimate the equivalent ISC resistance value.

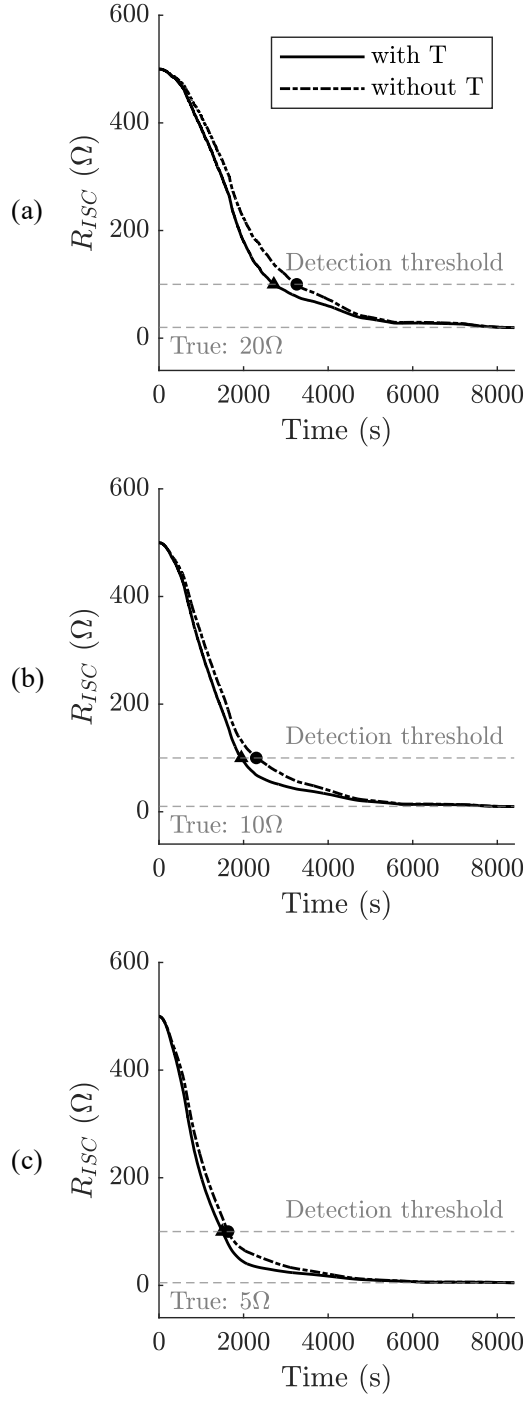

Figure 6. Timeliness performance comparison between the filter with only voltage and the filter with combined voltage and temperature measurements. The black triangle and circle indicate when the alarm is triggered for the two cases, respectively. The detection time saved for the different ISC severities is as follows: (a) Soft ISC: -20% (b) Moderate ISC: -18% (c) Severe ISC: -9%.

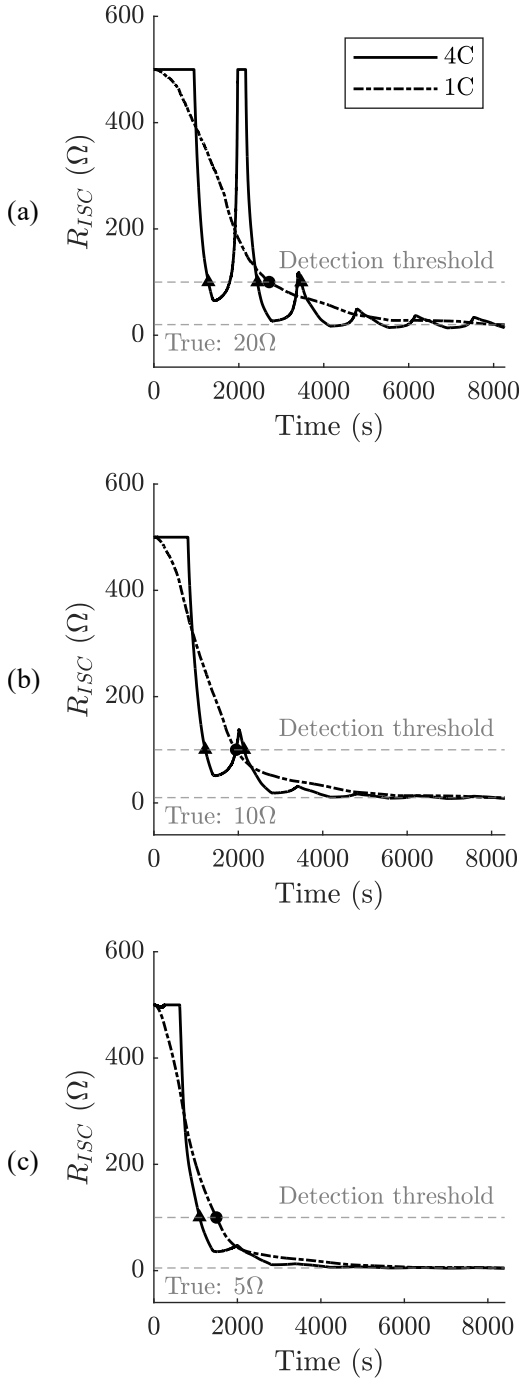

Figure 7. ISC detection results for different ISC conditions: 4C discharging/charging vs 1C discharging/charging. The black triangle and circle indicate when the alarm is triggered for the case of 4C and 1C, respectively. (a) Soft ISC (b) Moderate ISC (c) Severe ISC.

A further analysis of the detection results is conducted, this time considering different ambient temperatures at the different load conditions (high and low current, respectively). This is done in order to ascertain the extent to which environmental uncertainties affect the dynamics coupling in the plant and subsequently the detection performance for a fixed moderate ISC condition in the plant. The coupling between the thermal and electrical dynamics of a battery cell may become more or less strong, depending on the temperature difference between the cell core and the cell surface. This, in turn, is affected by the ambient temperature. The detection results at different ambient temperatures, considering an initial homogeneous temperature distribution in the plant, are summarised in Figure 8. Once again, the filter is capable of converging to a steady-state value of the equivalent ISC resistance, with an exception made for the case of 1C load current cycling at 5°C ambient temperature. Here, it is possible to make similar considerations regarding the fluctuations in the filter estimate when different ambient temperatures are considered, which increases the chances of triggering false alarms, penalizing the detection performance of the algorithm, and ultimately making it unstable.

The computational time required at each step of the online estimation has also been calculated in order to demonstrate the applicability of the approach in real-time. The real-time performance has been evaluated by computing the latency at each time step, that is the time taken for the algorithm to process a single unit of data from input to output. The average latency value is approximately 35 ms, with peak values of 50 ms for some spare time steps. These performances were obtained on a machine equipped with an Intel Core i7-9700 processor, with eight cores and 3.00 GHz, 64 GB of RAM, and a solid-state drive. It is notable that only approximately 10% of the CPU power is used (i.e., only one core of the processor) while running the algorithm. This indicates that a less powerful and cheaper processor can be used to run the algorithm in a BMS. In commercial BMS the latency typically ranges from 1s to 100ms (Kong et al., 2017). However, the latter latency range is typically required with respect to control applications. In contrast, for the considered application, namely monitoring and reporting, even higher latency values can be accepted. In conclusion, the results demonstrate the computational efficiency of the approach and its feasibility in terms of real-time implementation in a commercial BMS.

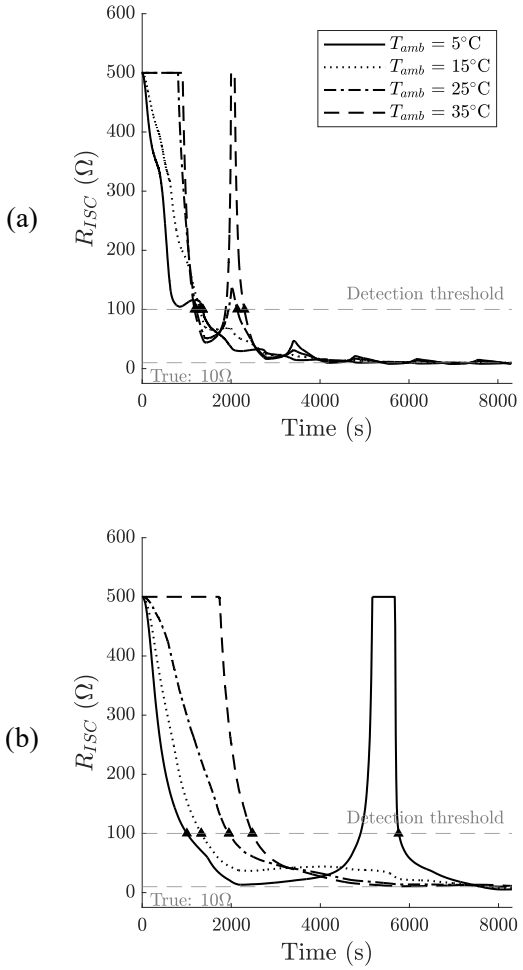

Figure 8. ISC detection results for a fixed moderate ISC condition in the plant with variable ambient temperature. The black triangle indicates when an alarm is triggered. (a) 4C load current cycling (b) 1C load current cycling.

5. CONCLUSION

This paper proposes a novel model-based approach for ISC detection in LIB cells. The method employs a computationally efficient model and a lean online state-estimation algorithm, which could be seamlessly integrated into a BMS to enhance battery cell management and safety. The approach is tested numerically considering a high-fidelity plant consisting of a coupled electro-thermal model of a cylindrical

battery cell. The plant model considers a second-order ECM model and a two-state thermal model to accurately mimic the electrical and thermal dynamics of the cell. By exploiting both surface temperature and the terminal voltage observations, the EKF algorithm can accurately estimate a state of its model that is directly related to the ISC condition of the plant. The satisfactory results of the detection process have demonstrated that, for different load conditions and ambient temperatures, the algorithm is capable of detecting ISC occurrence and also accurately quantifying its severity in a relatively short amount of time, that is approximately four working cycles. Therefore, we have demonstrated the robustness and reliability of the filtering algorithm proposed for effective ISC detection and quantification under different load conditions and environmental uncertainties. It is worth noting that detection performance could be further improved by incorporating dynamic coupling into the filter model, although this would require additional experimental analysis for accurate modelling and additional computing power to run the algorithm online. However, this may not be necessary if the battery is operated in a controlled environment and load, due to the presence of the battery and thermal management systems.

There are limitations to this study that require further investigation in future research. In this study, a single battery cell is considered, assuming that it is possible to access both surface temperature, voltage, and applied current for the single cell. In many applications, cells are typically stacked in modules, which in turn are arranged to form a battery pack. Consequently, future research will concentrate on developing model-based algorithms that are capable of detecting and potentially quantifying ISC occurrences in a battery pack, even when a limited network of temperature and voltage sensors is available.

ACKNOWLEDGMENT

The author Yiqi Jia would like to thank the China Scholarship Council for the financial support (CSC, No.202108320086).

REFERENCES

Amine, K., Kanno, R., & Tzeng, Y. (2014). Rechargeable lithium batteries and beyond: Progress, challenges, and future directions. *MRS Bulletin*, *39*(5), 395–401. doi: 10.1557/mrs.2014.62

Asakura, J., Nakashima, T., Nakatsuji, T., & Fujikawa, M. (2010). *Battery internal short-circuit detecting device and method, battery pack, and electronic device system* (No. US20100188054A1).

Asakura, J., Nakashima, T., Nakatsuji, T., & Fujikawa, M. (2012). *Battery internal short-circuit detection apparatus and method, and battery pack* (No. US8334699B2).

Bernardi, D., Pawlikowski, E., & Newman, J. (1985). A general energy balance for battery systems. *Journal of the electrochemical society*, *132*(1), 5. doi: 10.1149/1.2113792

Chang, W.-Y. (2013). The state of charge estimating methods for battery: A review. *International Scholarly Research Notices*, *2013*. doi: https://doi.org/10.1155/2013/953792

Feng, X., He, X., Lu, L., & Ouyang, M. (2018). Analysis on the Fault Features for Internal Short Circuit Detection Using an Electrochemical-Thermal Coupled Model. *Journal of The Electrochemical Society*, *165*(2), A155–A167. doi: 10.1149/2.0501802jes

Feng, X., Ouyang, M., Liu, X., Lu, L., Xia, Y., & He, X. (2018). Thermal runaway mechanism of lithium ion battery for electric vehicles: A review. *Energy Storage Materials*, *10*, 246-267. doi: https://doi.org/10.1016/j.ensm.2017.05.013

Gao, W., Li, X., Ma, M., Fu, Y., Jiang, J., & Mi, C. (2021). Case study of an electric vehicle battery thermal runaway and online internal short-circuit detection. *IEEE Transactions on Power Electronics*, *36*(3), 2452-2455. doi: 10.1109/TPEL.2020.3013191

Goodenough, J. B., & Kim, Y. (2010). Challenges for rechargeable Li batteries. *Chemistry of Materials*, *22*(3), 587–603. doi: 10.1021/cm901452z

Grabow, J., Klink, J., Orazov, N., Benger, R., Hauer, I., & Beck, H. P. (2023). Triggering and Characterisation of Realistic Internal Short Circuits in Lithium-Ion Pouch Cells—A New Approach Using Precise Needle Penetration. *Batteries*, *9*(10). doi: 10.3390/batteries9100496

Gu, W., & Wang, C. (2000). Thermal-electrochemical modeling of battery systems. *Journal of The Electrochemical Society*, *147*(8), 2910. doi: 10.1149/1.1393625

Jia, Y., Brancato, L., Giglio, M., & Cadini, F. (2024). Temperature enhanced early detection of internal short circuits in lithium-ion batteries using an extended kalman filter. *Journal of Power Sources*, *591*, 233874. doi: https://doi.org/10.1016/j.jpowsour.2023.233874

Kong, X., Zheng, Y., Ouyang, M., Li, X., Lu, L., Li, J., & Zhang, Z. (2017). Signal synchronization for massive data storage in modular battery management system with controller area network. *Applied Energy*, *197*, 52-62. doi: https://doi.org/10.1016/j.apenergy.2017.04.002

Kong, X., Zheng, Y., Ouyang, M., Lu, L., Li, J., & Zhang, Z. (2018). Fault diagnosis and quantitative analysis of micro-short circuits for lithium-ion batteries in battery packs. *Journal of Power Sources*, *395*, 358–368. doi: https://doi.org/10.1016/j.jpowsour.2018.05.097

Lai, X., Jin, C., Yi, W., Han, X., Feng, X., Zheng, Y., & Ouyang, M. (2021). Mechanism, modeling, detection, and prevention of the internal short circuit in lithium-ion batteries: Recent advances and perspec-

tives. *Energy Storage Materials*, *35*, 470-499. doi: https://doi.org/10.1016/j.ensm.2020.11.026

Lin, X., Perez, H. E., Mohan, S., Siegel, J. B., Stefanopoulou, A. G., Ding, Y., & Castanier, M. P. (2014). A lumped-parameter electro-thermal model for cylindrical batteries. *Journal of Power Sources*, *257*, 1-11. doi: https://doi.org/10.1016/j.jpowsour.2014.01.097

Lin, X., Perez, H. E., Siegel, J. B., Stefanopoulou, A. G., Li, Y., Anderson, R. D., ... Castanier, M. P. (2012). Online parameterization of lumped thermal dynamics in cylindrical lithium ion batteries for core temperature estimation and health monitoring. *IEEE Transactions on Control Systems Technology*, *21*(5), 1745–1755. doi: 10.1109/TCST.2012.2217143

Liu, G., Lu, L., Fu, H., Hua, J., Li, J., Ouyang, M., ... Chen, P. (2014). A comparative study of equivalent circuit models and enhanced equivalent circuit models of lithium-ion batteries with different model structures. In *2014 ieee conference and expo transportation electrification asia-pacific (itec asia-pacific)* (p. 1-6). doi: 10.1109/ITEC-AP.2014.6940946

Liu, X., Li, Y., Kang, Y., Zhao, G., Duan, B., & Zhang, C. (2024). An accurate co-estimation of core temperature and state of charge for lithium-ion batteries with electrothermal model. *IEEE Journal of Emerging and Selected Topics in Power Electronics*, *12*(1), 231-241. doi: 10.1109/JESTPE.2023.3304754

Ma, R., Deng, Y., & Wang, X. (2023). Simplified electrochemical model assisted detection of the early-stage internal short circuit through battery aging. *Journal of Energy Storage*, *66*(March). doi: 10.1016/j.est.2023.107478

Naha, A., Khandelwal, A., Agarwal, S., Tagade, P., Hariharan, K. S., Kaushik, A., ... Oh, B. (2020). Internal short circuit detection in Li-ion batteries using supervised machine learning. *Scientific Reports*, *10*(1), 1–10. doi: 10.1038/s41598-020-58021-7

Nise, N. S. (2020). *Control systems engineering*. John Wiley & Sons.

Park, C., & Jaura, A. K. (2003). *Dynamic thermal model of li-ion battery for predictive behavior in hybrid and fuel cell vehicles* (Tech. Rep.). SAE Technical Paper.

Qin, P., Che, Y., Li, H., Cai, Y., & Jiang, M. (2022). Joint soc–sop estimation method for lithium-ion batteries based on electro-thermal model and multi-parameter constraints. *Journal of Power Electronics*, *22*(3), 490–502.

Saqli, K., Bouchareb, H., M'sirdi, N. K., & Bentaie, M. O. (2023). Lithium-ion battery electro-thermal modelling and internal states co-estimation for electric vehicles. *Journal of Energy Storage*, *63*, 107072.

Seo, M., Park, M., Song, Y., & Kim, S. W. (2020). Online Detection of Soft Internal Short Circuit in Lithium-Ion Batteries at Various Standard Charging Ranges. *IEEE Access*, *8*, 70947–70959. doi: 10.1109/ACCESS.2020.2987363

Simon, D. (2006). *Optimal state estimation: Kalman, h infinity, and nonlinear approaches*. John Wiley & Sons.

Sun, C.-C., Chou, C.-H., Shieh, D.-T., & Chu, C.-W. (2021, March 16). *Battery safety identifying method and method for setting hazard levels of battery internal short circuit and warning system using the same.* Google Patents. (US Patent 10,948,544)

Walcott, B., & Zak, S. (1987). State observation of nonlinear uncertain dynamical systems. *IEEE Transactions on Automatic Control*, *32*(2), 166-170. doi: 10.1109/TAC.1987.1104530

Xiao, B., & Xiao, B. (2021). A novel approach for internal short circuit prediction of lithium-ion batteries by random forest. *International Journal of Electrochemical Science*, *16*(4), 210463. doi: https://doi.org/10.20964/2021.04.21

Zhang, G., Wei, X., Tang, X., Zhu, J., Chen, S., & Dai, H. (2021). Internal short circuit mechanisms, experimental approaches and detection methods of lithium-ion batteries for electric vehicles: A review. *Renewable and Sustainable Energy Reviews*, *141*(January). doi: 10.1016/j.rser.2021.110790

Zhang, J., Zhou, Z., & Huang, X. (2018). The application of ekf in parameter identification of state-space model. In *2018 eighth international conference on instrumentation measurement, computer, communication and control (imccc)* (p. 798-802). doi: 10.1109/IMCCC.2018.00171

Zhang, M. X., Du, J. Y., Liu, L. S., Siegel, J., Lu, L. G., He, X. M., & Ouyang, M. G. (2018). Internal short circuit detection method for battery pack based on circuit topology. *Science China Technological Sciences*, *61*(10), 1502–1511. doi: 10.1007/s11431-017-9299-3

BIOGRAPHIES

Yiqi. JIA was born in China on January 28, 1996. She holds a Bachelor's degree in Automotive Engineering from Wuhan University of Technology, Wuhan, China (2017), and a Master's degree in Automotive Engineering from the University of Bath, Bath, UK (2018). After working as a vehicle engineer for nearly 3 years at Ford Motor Company, she started her Ph.D. journey in Mechanical Engineering at Politecnico di Milano in November 2021. Her research primarily focuses on the diagnosis and prognosis of Lithium-ion batteries, structural batteries, and more broadly, on mechanical/structural-related behaviours. This includes battery modeling, simulation, and data-based estimation methods for optimal battery management.

Lorenzo. BRANCATO was born in Italy on December 12, 1998. He earned his Bachelor's degree in Mechanical Engineering from Politecnico di Milano in 2020. Subsequently, he pursued a Master's degree in Mechatronic Engineering at Politecnico di Milano, completing his studies in 2022. He has started his Ph.D in Mechanical Engineering at Politecnico di Milano in 2023. His current research focus on the development of advanced diagnostic and prognostic approaches for dynamic, complex systems subject to degradation. This involves high-fidelity multi-physics modeling, simulation and advanced model-based filtering methods.

Marco. GIGLIO is Full Professor at the Department of Mechanical Engineering, Politecnico di Milano. His main research fields are: (i) Structural integrity evaluation of complex platforms through Structural Health Monitoring methodologies; (ii) Vulnerability assessment of ballistic impact damage on components and structures, in mechanical and aeronautical fields; (iii) Calibration of constitutive laws for metallic materials; (iv) Expected fatigue life and crack propagation behaviour on aircraft structures and components; (v) Fatigue design with defects. He has been the coordinator of several European projects: HECTOR, Helicopter Fuselage Crack Monitoring and prognosis through on-board sensor, 2009-2011, ASTYANAX (Aircraft fuselage crack Monitoring System and Prognosis through eXpert onboard sensor networks), 2012-2015, and SAMAS (SHM application to Remotely Piloted Aircraft Systems), 2018-2020. He has been the project leader of the Italian Ministry of Defence project in the National Plan of Military Research, SUMO (Development of a predictive model for the ballistic impact), 2011-2012 and, SUMO 2 (Development of an analytical, numerical and experimental methodology for design of ballistic multilayer protections), 2017-2019. He has published more than 210 papers, h-index 27 (source Scopus) in referred international journals and congresses.

Francesco. CADINI (MSc in Nuclear Engineering, Politecnico di Milano, 2000; MSc in Aerospace Engineering, UCLA, 2003; PhD in Nuclear Engineering, Politecnico di Milano, 2006) is Associate Professor at the Department of Mechanical Engineering, Politecnico di Milano. He has more than 20 years of experience in the assessment of the safety and integrity of complex engineering systems, entailing (i) artificial intelligence (machine learning)-based approaches for classification and regression, (ii) development and application of advanced Monte Carlo algorithms for reliability analysis (failure probability estimation), (iii) diagnosis and prognosis (HUMS) of dynamic, complex systems subject to degradation, (iv) uncertainty and sensitivity analyses, (v) structural reliability analyses.